Slip model of the 2015 M_w 7.8 Gorkha (Nepal) earthquake from inversions of ALOS-2 and GPS data

Kang Wang[1] and Yuri Fialko[1]

[1] Institute of Geophysical and Planetary Physics, Scripps Institution of Oceanography, University of California, San Diego, La Jolla, California, USA

Abstract We use surface deformation measurements including Interferometric Synthetic Aperture Radar data acquired by the ALOS-2 mission of the Japanese Aerospace Exploration Agency and Global Positioning System (GPS) data to invert for the fault geometry and coseismic slip distribution of the 2015 M_w 7.8 Gorkha earthquake in Nepal. Assuming that the ruptured fault connects to the surface trace of the Main Frontal Thrust (MFT) fault between 84.34°E and 86.19°E, the best fitting model suggests a dip angle of 7°. The moment calculated from the slip model is 6.08×10^{20} Nm, corresponding to the moment magnitude of 7.79. The rupture of the 2015 Gorkha earthquake was dominated by thrust motion that was primarily concentrated in a 150 km long zone 50 to 100 km northward from the surface trace of the Main Frontal Thrust (MFT), with maximum slip of ~ 5.8 m at a depth of ~ 8 km. Data thus indicate that the 2015 Gorkha earthquake ruptured a deep part of the seismogenic zone, in contrast to the 1934 Bihar-Nepal earthquake, which had ruptured a shallow part of the adjacent fault segment to the east.

1. Introduction

The M_w 7.8 Gorkha (Nepal) earthquake occurred on 25 April 2015 in the central Himalaya, on a tectonic boundary resulted from the India-Eurasia collision. It caused more than 8000 fatalities and was the largest seismic event since the 1956 Assam-Tibet Nepal M_w 8.6 earthquake along Himalayan arc [*Bilham et al.*, 2001]. The centroid moment tensor (CMT) solution and preliminary finite fault inversions of seismic data suggested that the earthquake rupture occurred along a NWW trending fault with a primarily thrust mechanism and a minor component of dextral slip. Both the CMT solution and seismically determined finite fault models indicate that the dip angle of the fault is small (e.g., 7° in global CMT solution (iris.edu, Moment tensor for MW 7.9 (GCMT) NEPAL, 2015, http://ds.iris.edu/spud/momenttensor/9925741, Accessed 30 June 2015) and 10° in the U.S. Geological Survey determined finite fault model (earthquakes.usgs.gov, Earthquake hazard program, 2015, http://earthquake.usgs.gov/earthquakes/eventpage/us20002926#general_summary, Accessed 30 June 2015)). Geologically, the most active structure along the Himalayan arc is the Main Himalayan Thrust (MHT) fault, which reaches the surface at Main Frontal Thrust fault (MFT), and absorbs about 20 mm/yr of the India-Eurasia convergence in Nepal [*Lavé and Avouac*, 2000]. Analysis of GPS measurements before the M_w 7.8 Nepal earthquake indicates that the MFT is locked from surface to a distance of approximately 100 km downdip [*Ader et al.*, 2012]. Most of the aftershocks of the 2015 event are located at least 30 km north of the MFT, suggesting that if the earthquake occurred along the MHT, it may not have ruptured the shallow part of the fault. It has been suggested that the MFT can be viewed as one of the splays of thrust faults rooting in a midcrustal décollement [e.g., *Pandey et al.*, 1999; *Avouac*, 2003; *Ader et al.*, 2012]. However, the geometry of the décollement (in particular, its dip angle) is not well known. In this paper, we use observations of surface deformation from Global Positioning System (GPS) and synthetic aperture radar (SAR) collected by ALOS-2 satellite of the Japanese Space Agency to derive the slip distribution due to the 2015 M_w 7.8 Gorkha earthquake and constrain the geometry of the earthquake rupture.

2. Data and Methods

The data used in the inversion include vector displacements measured at 13 GPS stations and line-of-sight (LOS) displacements derived from synthetic aperture radar (SAR) data from three tracks of the ALOS-2 satellite (Figure 1). The raw GPS data are from the network deployed by the Caltech Tectonics Observatory and processed by Advanced Rapid Imaging and Analysis Center for Natural Hazards at Jet Propulsion Laboratory [*Galetzka et al.*, 2015]. Both horizontal and vertical components of the GPS displacements were used in the
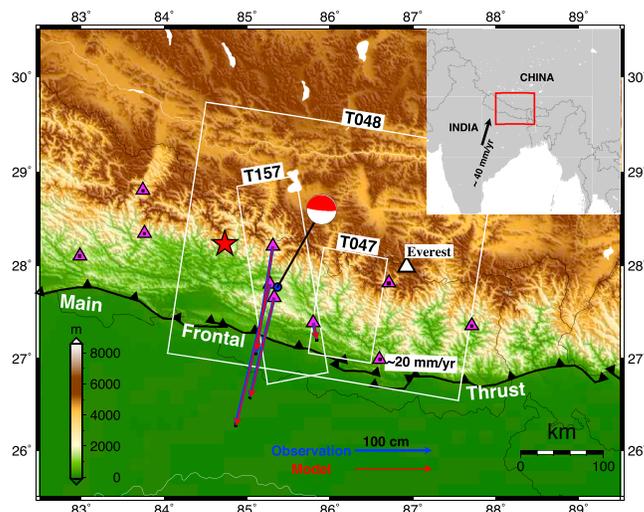
Figure 1. Tectonic setting of 25 April 2015 M_w 7.8 Nepal earthquake. Thick black line represents the surface trace of the Main Frontal Thrust (MFT) [*Ader et al.*, 2012]. The red star denotes the epicenter (earthquakes.usgs.gov, online report, 2015), and the beach ball denotes the centroid moment tensor (iris.edu, online report, 2015) of the M_w 7.8 main shock. White boxes show the coverage of ALOS-2 data (ascending track T157, descending track T048, and fifth subswath of descending track T047). Blue and red arrows represent the observed and modeled horizontal surface displacements at GPS sites (magenta triangles).

inversion. ALOS-2 data were processed using GMTSAR [*Lindsey et al.*, 2015]. The unwrapped InSAR phase was detrended by removing a linear ramp estimated from far-field LOS displacements for each track to account for possible orbital errors and/or ionosphere variations. InSAR data were downsampled using a recursive algorithm that enables denser sampling in areas of larger gradients in LOS displacements [*Simons et al.*, 2002; *Fialko*, 2004]. To avoid oversampling in areas with large phase gradients due to noise (atmospheric delays, decorrelation, unwrapping errors, etc.), our downsampling of the InSAR data was implemented iteratively using model predictions [e.g., *Lohman and Simons*, 2005]. An initial slip model was estimated from inversion of coarsely sampled LOS displacement maps. Synthetic interferograms were computed using the slip model and downsampled using the quad-tree curvature-based algorithm. The bounding coordinates of each resolution cell (bin) were then used to compute the average LOS displacements from the observed interferograms. A new slip model was then derived from the updated data set. Usually, a few iterations are sufficient to achieve a solution that stops changing with subsequent iterations. To avoid spurious shallow slip, a relatively dense sampling around the fault trace was retained through all iterations (see Figure S1 in the supporting information for the final downsampling of the InSAR measurements in this study). The radar incidence angles were computed by averaging the original values in respective resolution cells.

Our kinematic inversions assumed that fault slip can be approximated by a superposition of rectangular dislocations in a homogeneous elastic half-space [*Okada*, 1985]. The fault geometry was constrained by the assumption that the rupture plane intersects the surface along the MFT between 84.34°E and 86.19°E. The ~185 km long and 160 km wide fault was divided into patches which sizes gradually increase with depth to ensure a relatively uniform model resolution [e.g., *Fialko*, 2004]. Each individual patch was allowed to have a thrust and a right-lateral slip component of up to 10 m. Laplacian smoothing was applied between adjacent fault patches to avoid abrupt variations in slip. We further regularized the inversion problem by requiring no slip at the fault edges (except at the surface). We determined the optimal values of smoothness of the model and relative weighting between GPS and InSAR LOS data as described by *Wang and Fialko* [2014] (also see Figures S2 and S3 in the supporting information).

The initial inversions were performed assuming a dip angle of 10°. However, we found that the best fitting model failed to provide a good fit to data from the ascending and descending tracks (T147 and T048) simultaneously, regardless of what model parameters (e.g., degree of smoothing or relative weighting between GPS and InSAR data sets) were chosen. We then allowed the dip angle to vary in the range of 1° – 15° and solved
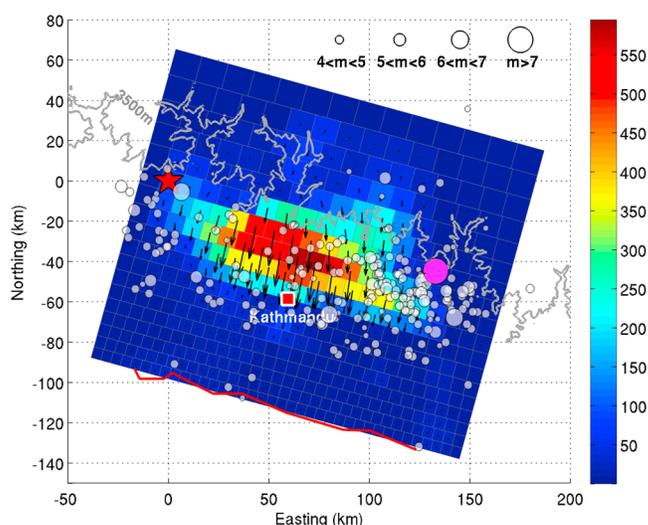
Figure 2. Surface projection of the coseismic slip model of 25 April M_w 7.8 Gorkha earthquake. Red line represents the surface trace of MFT used to constrain the strike of the fault plane. Red star denotes the epicenter of the M_w 7.8 main shock. Gray dots denote the aftershocks of $m > 4$ from 25 April to 31 May 2015. The M_w 7.3 aftershock on 12 May 2015 is shown by a magenta circle. Color shows the slip magnitude in centimeters, and arrows correspond to the slip directions. The gray line represents the surface elevation of 3500 m. Red square denotes the city of Kathmandu. The origin corresponds to the epicenter of the main shock (84.731°E, 28.230°N).

for the slip distribution for each assumed geometry. For each run, we quantified the misfit between the model and the data by calculating

$$\chi^2 = \frac{1}{N} \sum_{i=1}^{N} \left(\frac{d_i - d_i'}{\sigma_i} \right)^2 \tag{1}$$

where d and d' represent vectors of observations and model predictions, respectively; σ represents the corresponding uncertainty for each data set (LOS displacements from three ALOS-2 tracks and horizontal and vertical displacements at 13 GPS sites); and N is the length of the data vector. Uncertainties in InSAR data were estimated by computing the variation of the LOS displacements in the far field of each interferogram, where the deformation due to earthquake is expected to be negligible. The estimated root-mean-square (RMS) of the LOS displacements in the far field are 2.3, 5.4, and 4.1 cm for tracks T047, T048, and T157, respectively. We note that the variation estimated this way only provides a qualitative measure of accuracy of the InSAR measurements and does not reflect the uncertainty of individual data points. The GPS uncertainties are computed as part of the GPS solutions and are mostly < 3 mm for horizontal components and < 1 cm for vertical component.

3. Results

We found that a model with a dip angle of 7° fits the LOS displacements from of all three ALOS-2 tracks as well as GPS data very well, with a low misfit of $\chi^2 = 1.1561$ (see Figure S4 in the supporting information). The preferred coseismic slip model is shown in Figure 2. The model is characterized by dominantly thrust slip, with minor contribution of dextral component, concentrated in a relatively narrow (compared to the along-strike rupture dimension) zone between ~50 and ~100 km along the downdip direction. The maximum slip is ~ 5.8 m at a depth of ~ 8 km with respect to sea level. The total moment is 6.08×10^{20} Nm, corresponding to a moment magnitude of $M_w = 7.79$, in excellent agreement with the seismic moment (earthquakes.usgs.gov, online report, 2015). The slip on the central part of the rupture seems to have extended farther downdip, compared to both the eastern and western tips of the rupture that appear to taper to a width of 20–30 km (see Figures 2 and 5). Most of the aftershocks occurred along the eastern half of the fault, around the patches of relatively large coseismic slip, including the M_w 7.3 aftershock on 12 May 2015 (magenta circle in Figure 2).

Figure 3 shows a comparison of the ALOS-2 data with predictions of the best fitting slip model (Figure 2). The model is able to reproduce InSAR measurements from all three tracks (Figure 3) as well as GPS measurements
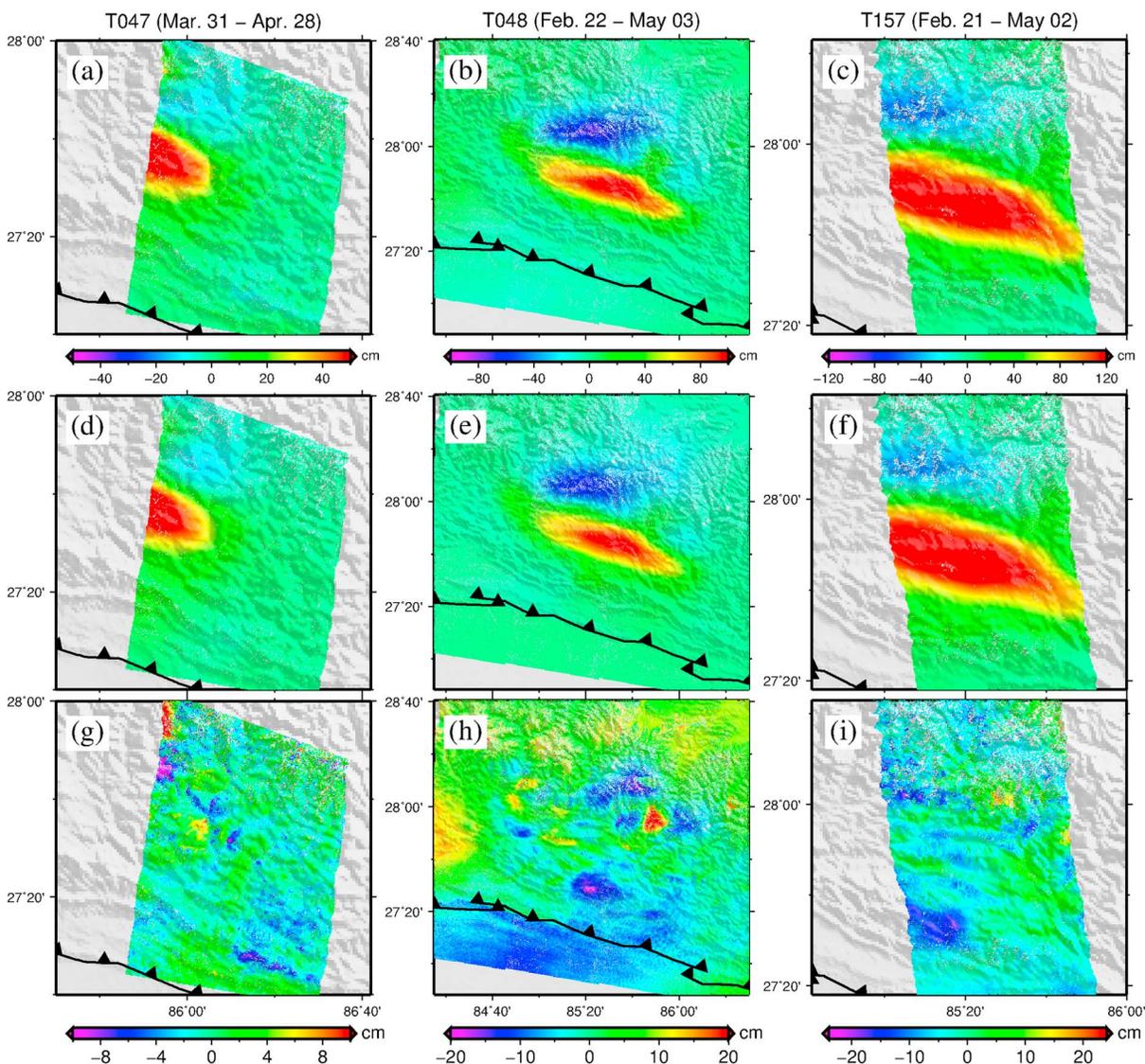
Figure 3. Comparison of observed and modeled LOS displacements from three ALOS-2 tracks. The forward calculation is based on a model assuming a planar fault with the dip angle of 7° that intersects the surface at the trace of MFT (Figure 2). (a–c) Observations, (d–f) model predictions, and (g–i) residuals. Note the differences in color scales between the data/models and the residuals. Subtitles denote the track numbers and SAR acquisition dates (in parentheses; all in year 2015).

(Figures 1 and S5). Interestingly, a comparison with a coseismic interferogram made using Sentinel-1 data shows that the latter underpredicts the amplitude of the LOS displacements by as much as 50% (supporting information Figure S7), likely due to a trade-off between the estimation of a burst alignment and range changes intrinsic to the TOPS mode of Sentinel-1.

It was suggested that the MHT geometry involves two ramp-flats, with the top flat lying at ~5 to 10 km depth [*Avouac*, 2003]. To allow for listric (curved) fault geometry, we performed another set of inversions in which the fault surface was parameterized as

$$z = -\frac{2a}{\pi} \arctan \frac{y}{b} \qquad (2)$$

where z is the depth of the fault at a distance of y from the surface trace (i.e., MFT) and a and b are geometric parameters that were varied in the inversion. Specifically, a represents the depth of the fault at infinite distance from the surface trace (corresponding to the depth of the flat in the ramp flat décollement system), while b controls the fault curvature near the surface (corresponding to the geometry of the ramp in the ramp
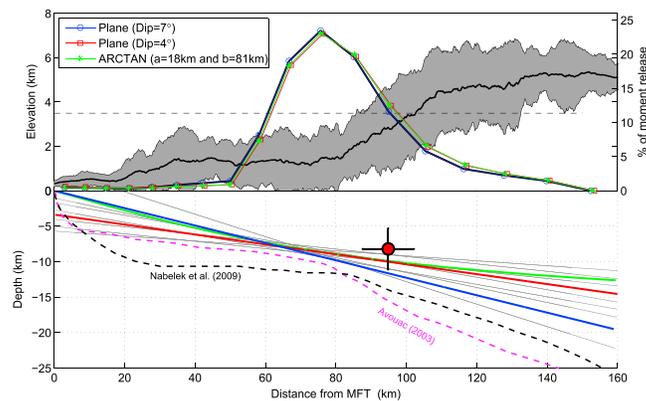
Figure 4. Comparison of slip models assuming planar and curved fault geometry. (a) Moment release and topography along dip direction. The shaded gray area shows the elevation variations along the direction normal to the average strike of MFT (285°) as marked by red line in Figure 2. The blue, red, and green lines show the percentages of moment release as a function of distance from MFT for the three best fitting fault geometries. (b) Geometries of the fault models at depth (blue for planar fault of dip angle of 7° that intersects the surface at MFT, green for curved fault approximated by an arctan function, red for planar fault with dip angle of 4°). Thin gray lines represent the geometries of planar faults yielding low misfits (see Figure S6). The red circle with error bars represents the hypocentral depth of the main shock. The dashed black and magenta lines denote the geometries of MHT inferred by *Nábělek et al.* [2009] and *Avouac* [2003], respectively.

flat décollement system). A planar fault is a particular case of equation (2), given sufficiently large b. Using the same parameters for smoothness and relative weighting between data sets as before, we inverted for the slip distribution on a curve fault described by equation (2) for a range of values of $a \in [1 : 1 : 30]$ km and $b \in [1 : 10 : 300]$ km. The slip model yields the lowest misfit of $\chi^2_{\text{curved}} = 1.0349$ for $a = 18$ km and $b = 81$ km. This can be compared with $\chi^2_{\text{planar}} = 1.1561$ for the case of a planar fault, suggesting that a ramp-flat décollement model is in better agreement with surface deformation data. The overall slip distribution based on the curved fault is quite similar to that of a planar fault with a dip angle of 7° (Figure 2). The two models are very similar down to depth of 10 km, where most of coseismic slip occurred (Figure 4). We also ran a suite of inversions in which we relaxed the assumptions that the fault plane intersects the surface at the trace of MFT. In these inversions, the fault strike was fixed at 285°, and the fault was required to go through an assumed hypocenter. Because the hypocenter depth is only approximately constrained by seismic data, we allowed it to vary between 4 and 20 km. The fault dip was allowed to vary between 1 to 15°. The model
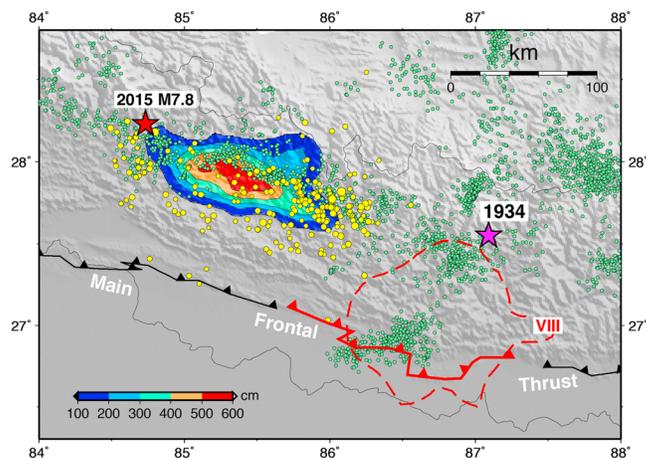

Figure 5. Spatial relationship between the 2015 M_w 7.8 Gorkha earthquake and the 1934 M_w 8.6 Bihar-Nepal earthquake. Color represents the coseismic slip of the 2015 event. Yellow dots denote the aftershocks of the 2015 event from April 25, 2015 to May 31 2015. Light green dots denote the background seismicity from 1995 to 2002 [*Ader et al.*, 2012]. Red solid and dashed lines represent the inferred rupture segment and the isoseismal intensity of VIII of the 1934 Bihar-Nepal earthquake, respectively [*Sapkota et al.*, 2013]. Magenta star denotes the relocated epicenter of the 1934 event [*Chen and Molnar*, 1977].

misfits are shown in Figure S6, and the family of fault geometries that fit the data equally well are shown by gray lines in Figure 4. The respective slip distribution is quite similar to that of the planar fault that intersects the surface at the location of MFT. The best fitting geometries are close to subsurface geometries of the MHT suggested by previous studies [*Avouac*, 2003; *Nábělek et al.*, 2009]. Somewhat shallower depths of the geodetic models compared to the inferred geometries of the MHT (Figure 4) might be attributed to the neglect of increases in elastic rigidity with depth [e.g., *Fialko*, 2004]. However, we note that the seismically determined origin depth is in better agreement with the best fitting geodetic models than with the previously suggested geometry of the MHT (Figure 4). The geodetically inferred dip angles are, in fact, an upper bound, as model does not take into account surface topography. The average slope due to topography across the MHT is 2 to 5°(Figure 4), and a half-space model is expected to bias the dip angle (measured with respect to the horizontal) by a value of the order of the topographic slope. More sophisticated simulations that take into account surface topography are needed to refine the slip model of the 2015 Gorkha earthquake.

4. Discussion

Seismicity along the Himalayan arc is known to occur along a relatively narrow zone which follows the front of high Himalaya and tends to shut off underneath the higher Himalaya (elevations higher than 3500 m, see the gray line in Figure 2) [e.g., *Pandey et al.*, 1995, 1999; *Avouac*, 2003]. The coseismic slip due to the 2015 M_w 7.8 Nepal earthquake is also concentrated in a fairly narrow zone (between ~50 and ~100 km) from the MFT at the deep end of the seismogenic zone. The extent of interseismic locking at ~100 km north of the MFT likely marks the brittle-ductile transition and changes in rate dependence of friction due to the elevated pressure and temperature.

Our slip model shows that the 2015 rupture did not propagate into shallow part of the MHT. Analysis of GPS measurements made before the earthquake indicates that the MHT is locked from surface to a distance of approximately 100 km downdip [*Ader et al.*, 2012]. Recent investigations of the Quaternary geomorphology along the MFT showed that at least two great earthquakes had ruptured to the surface in Nepal in the past 1000 years [*Sapkota et al.*, 2013]. Particularly, the 1934 Bihar-Nepal *M* 8.2 earthquake ruptured a ~ 150 km long segment of the MFT between 85.8°E and 87.3°E, immediately to the east of the 2015 rupture (Figure 5). Unless the degree of seismic coupling varies along the fault strike, the lack of shallow slip during the 2015 Gorkha earthquake implies future seismic hazard, in particular, because this part of the fault has been brought closer to failure by the 2015 earthquake. Observations of postseismic deformation (in particular, the occurrence of afterslip on the upper section of the MFT) will provide important constraints on the degree of seismic coupling and seismic hazard on this part of this fault.

5. Conclusions

We used the surface displacement data provided by GPS and InSAR to model the coseismic slip distribution and fault the geometry of the 2015 M_w 7.8 Gorkha earthquake in Nepal. Aftershocks of the 2015 event were mostly surrounding the areas of high coseismic slip. The best fitting model suggests a shallow dip angle of 7° for the MHT. The 2015 Gorkha earthquake ruptured the deep part of the seismogenic zone, with little or no slip in the shallow part (within 50 km from the MFT). This is in contrast to the 1934 Bihar-Nepal event, whose rupture had likely reached the surface, implying increased seismic hazard on the fault section updip of the 2015 event.

References

Ader, T., et al. (2012), Convergence rate across the Nepal Himalaya and interseismic coupling on the Main Himalayan Thrust: Implications for seismic hazard, *J. Geophys. Res.*, *117*, B04403, doi:10.1029/2011JB009071.

Avouac, J.-P. (2003), Mountain building, erosion, and the seismic cycle in the Nepal Himalaya, in *Advances in Geophysics*, vol. 46, pp. 1–80, Elsevier, San Diego, Calif.

Bilham, R., V. K. Gaur, and P. Molnar (2001), Earthquakes: Himalayan seismic hazard, *Science*, *293*(5534), 1442–1444.

Chen, W.-P., and P. Molnar (1977), Seismic moments of major earthquakes and the average rate of slip in central Asia, *J. Geophys. Res.*, *82*(20), 2945–2969.

Fialko, Y. (2004), Probing the mechanical properties of seismically active crust with space geodesy: Study of the coseismic deformation due to the 1992 M_w 7.3 Landers (southern California) earthquake, *J. Geophys. Res.*, *109*, B03307, doi:10.1029/2003JB002756.

Galetzka, J., et al. (2015), Slip pulse and resonance of Kathmandu basin during the 2015 M_w 7.8 Gorkha earthquake, Nepal imaged with geodesy, *Science*, *349*(6252), 1091–1095, doi:10.1126/science.aac6383.

Lavé, J., and J.-P. Avouac (2000), Active folding of fluvial terraces across the Siwaliks Hills, Himalayas of central Nepal, *J. Geophys. Res.*, *105*(B3), 5735–5770.

Lindsey, E. O., R. Natsuaki, X. Xu, M. Shimada, M. Hashimoto, D. Melgar, and D. T. Sandwell (2015), Line-of-sight displacement from ALOS-2 interferometry: M_w 7.8 Gorkha Earthquake and M_w 7.3 aftershock, *Geophys. Res. Lett.*, *42*, 6655–6661, doi:10.1002/2015GL065385.

Lohman, R. B., and M. Simons (2005), Some thoughts on the use of InSAR data to constrain models of surface deformation: Noise structure and data downsampling, *Geochem. Geophys. Geosyst.*, *6*, Q01007, doi:10.1029/2004GC000841.

Nábělek, J., G. Hetényi, J. Vergne, S. Sapkota, B. Kafle, M. Jiang, H. Su, J. Chen, B.-S. Huang, and H.-C. Team (2009), Underplating in the Himalaya-Tibet collision zone revealed by the Hi-CLIMB experiment, *Science*, *325*(5946), 1371–1374.

Okada, Y. (1985), Surface deformation due to shear and tensile faults in a half-space, *Bull. Seismol. Soc. Am.*, *75*(4), 1135–1154.

Pandey, M. R., R. P. Tandukar, J. P. Avouac, J. Lavé, and J. P. Massot (1995), Interseismic strain accumulation on the Himalayan crustal ramp (Nepal), *Geophys. Res. Lett.*, *22*(7), 751–754.

Pandey, M. R., R. P. Tandukar, J. P. Avouac, J. Vergne, and T. Héritier (1999), Seismotectonics of the Nepal Himalaya from a local seismic network, *J. Asian Earth Sci.*, *17*(5-6), 703–712.

Sapkota, S. N., L. Bollinger, Y. Klinger, and P. Tapponnier (2013), Primary surface ruptures of the great Himalayan earthquakes in 1934 and 1255, *Nat. Geosci.*, *6*(2), 71–76.

Simons, M., Y. Fialko, and L. Rivera (2002), Coseismic deformation from the 1999 M_w 7.1 Hector Mine, California, earthquake as inferred from InSAR and GPS observations, *Bull. Seismol. Soc. Am.*, *92*(4), 1390–1402.

Wang, K., and Y. Fialko (2014), Space geodetic observations and models of postseismic deformation due to the 2005 M7.6 Kashmir (Pakistan) earthquake, *J. Geophys. Res. Solid Earth*, *119*, 7306–7318, doi:10.1002/2014JB011122.